Journal of Alloys and Compounds 989 (2024) 174254

Contents lists available at ScienceDirect

Journal of Alloys and Compounds

journal homepage: www.elsevier.com/locate/jalcom

Tailored nanofiber composites for a flexible piezoelectric nanogenerator: Poly(vinylidene fluoride) with $BaTiO_3/NiFe_2O_4$

Hemalatha Parangusan [a], K. Karuppasamy [b], Jolly Bhadra [a,*]

[a] Qatar University Young Scientists Center (QUYSC), Qatar University, Doha 2713, Qatar
[b] Department of Chemical and Petroleum Engineering, Khalifa University of Science and Technology, Abu Dhabi 127788, United Arab Emirates

ARTICLE INFO

Keywords:
$BaTiO_3/NiFe_2O_4$ nanocomposite
PVDF
Piezoelectric nanogenerator
Dielectrics

ABSTRACT

Owing to the depletion of fossil fuel energy and the pollution caused by chemical batteries, as well as the growing number of electronic devices and the Internet of Things (IoT), there is a greater demand for power devices that are lightweight, inexpensive, durable, and sustainable. An excellent alternative is a self-sufficient, adaptable piezoelectric energy harvester, easily integrated with small electronics to generate real-time, sustained energy. This study develops a piezoelectric nanogenerator (PENG) by uniformly drawing spun membranes containing 2 wt% of barium titanate ($BaTiO_3$) and nickel ferrite ($NiFe_2O_4$). The flexible piezoelectric nanogenerator was prepared by electrospinning technique. The electroactive phase content of PVDF is increased by adding nanofillers, and the interfacial polarization between the nanofiller and polymer matrix is significantly enhanced. The obtained electrospun nanofibers were evaluated for mechanical flexibility and piezoelectric responses. The findings demonstrated that, for a given filler composition, the output voltage achieved was more significant than the voltage generated by the pure PVDF. The PVDF/$BaTiO_3$-$NiFeO_4$ electrospun nanofibers demonstrated the highest piezoelectric peak-to-peak output voltage of 4.1 compared to pure PVDF (~125 mV). From these results, the prepared electrospun polymer nanocomposite fibers may be preferred as the energy-converting devices that can be applied to flexible and wearable electronics. The materials mechanical, breakdown strength and dielectric characteristics align with their potential uses in wearable electronics.

1. Introduction

The growing demand for energy resources for powerhouses and personal electronics has drawn attention to developing renewable energy sources. It has been demonstrated that using solar cells and converting mechanical vibrations into electrical energy are efficient methods of producing energy naturally [1,2]. Energy harvesting via mechanical vibrations has become more significant in recent years since small electronic components, including wireless sensor networks used in monitoring applications, require less power [3]. One method of producing electricity is developing transducers that can transition between electrical energy and mechanical strain or force using piezoelectric materials. These substances have the potential to function as mechanisms that convert ambient motion (generally vibration) into electrical energy that can be stored and utilized to power other electronics [4].

Due to their toxicity and brittleness, inorganic ceramics with good levels of piezo responsiveness, such as lead zirconate titanate (PZT), lead magnesium niobate-lead titanate (PMN-PT) and barium titanate ($BaTiO_3$), are not appropriate for flexible electronics and biomedical applications [5–8]. In contrast, readily available polyvinylidene fluoride (PVDF) and its copolymers are examples of flexible, biocompatible, low-cost, lightweight, and electroactive piezoelectric polymers. Increasing their piezoelectric properties becomes difficult due to their semicrystalline structure [9,10]. Semicrystalline PVDF is composed of α, β, γ, δ, and ϵ polymorphs. The electroactive phase (β, γ) is the most polar polymorph responsible for the high piezoelectric properties. To enhance the piezoelectric properties of PVDF, high-field electric polling is frequently used for β-phase nucleation. Nevertheless, this external electric poling technique is expensive, challenging to use, and unsuitable for large-scale manufacturing [11,12].

After cooling from the melt, PVDF and its copolymers generally have a small amount of polar β-phase. The polar phase has been stabilized and increased in the presence of fillers including clay, Fe_3O_4, ZrO_2, and $BaTiO_3$ [13–17]. The fillers outstanding compatibility and the PVDF matrixs effective interaction are the primary driving factors of the electroactive phases of PVDF-based composites. Research has

* Corresponding author.
E-mail address: jollybhadra@qu.edu.qa (J. Bhadra).

https://doi.org/10.1016/j.jallcom.2024.174254
Received 24 December 2023; Received in revised form 5 March 2024; Accepted 22 March 2024
Available online 22 March 2024

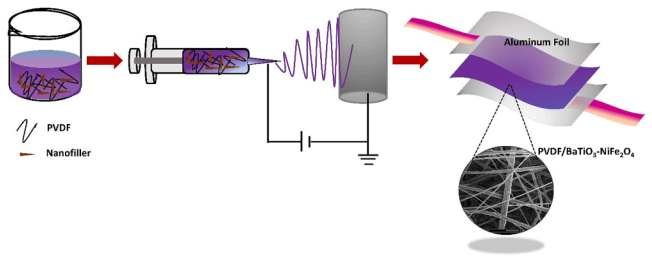

Fig. 1. A schematic illustration showing the process for producing PVDF/$BaTiO_3$-$NiFe_2O_4$ composites.

demonstrated that the α-to-β-phase transition of PVDF is facilitated by electrospinning, a flexible method for creating nanofibers with diameters from a few to several micrometers [18].

The size of the ceramic $BaTiO_3$ filler has been found to impact the electroactive phase of PVDF significantly. The formation of the ferroelectric phase should be primarily influenced by structural factors, including interactions at the interface between the PVDF dipoles and the local electric field. Various local field-dipole interactions, including dipole-dipole and ion-dipole interactions, can have different characteristics based on the nanofillers [19]. It is essential to understand the nanocomposites interfaces to generate materials with specific properties using this process. When ferrite nanoparticles are added to the material, this issue becomes of greater importance since the composite exhibits a magnetoelectric effect in addition to the electroactive phase nucleation, which has significant potential applications. Ferrite nanoparticles were shown to have an impact on the nucleation kinetics. This is confirmed by variations in Avrams exponent and the observation that the number of spherulites increased as the concentration of nanoparticles increased. In addition, the decrease in the crystalline percentage of PVDF observed with an increase in nanoparticle loading suggests that a significant portion of the polymer chains are trapped in interphases with the filler particle [20].

The current study reported the electrospun nanofibers-based piezoelectric nanogenerator with $NiFe_2O_4$ and piezoelectric $BaTiO_3$ nanoparticles. The output performance of the PVDF/$BaTiO_3$-$NiFe_2O_4$ piezoelectric nanogenerator was improved. The PVDF matrix contains a $BaTiO_3$/$NiFe_2O_4$ nanofiller, which generates an excellent piezoelectric property. Due to its flexibility, environmental friendliness, and economic viability, the flexible PVDF/$BaTiO_3$-$NiFe_2O_4$ piezoelectric nanogenerator exhibits tremendous potential of fabricating self-powered electronic devices and implantable or wearable energy harvesters.

2. Experimental method

2.1. Materials

Barium acetate ($C_4H_6BaO_4$), iron chloride ($FeCl_3.6\ H_2O$), nickel nitrate ($Ni(NO_3)_2.6\ H_2O$), and KOH were purchased from Sigma Aldrich. Titanium (IV) n-butoxide ($C_{16}H_{36}O_4$)Ti) was obtained from Fisher Scientific. Acetone, N, N-dimethylformamide (DMF) and PVDF (Polyvinylidene fluoride) pellets (Mw∼ 275,000 g/mol) were obtained from Sigma-Aldrich. Ethanol (C_2H_5OH) was purchased from Sigma Aldrich.

2.2. Synthesis of $BaTiO_3$/$NiFe_2O_4$ nanomaterial

$BaTiO_3$/$NiFe_2O_4$ composites were synthesized by using the hydrothermal method. In brief, deionized water was used to prepare 0.06 M of iron chloride and nickel nitrate solutions, which were then mechanically mixed. After dissolving titanium (IV) n-butoxide (0.04 M) in ethanol, barium acetate (0.04 M) was added. The above solutions were thoroughly mixed and agitated for two hours to produce a homogenous solution. By adding 0.1 M KOH solution, the pH was kept at 13. The solution was then heated to 180° C in a Teflon-lined steel autoclave for 32 hours. The resulting residue was rinsed with ethanol and distilled water then dried at 80° C for six hours.

2.3. Fabrication of PVDF/$BaTiO_3$-$NiFe_2O_4$ polymer nanocomposite fibers

The PVDF polymer was dissolved in a 1:1 solvent solution of DMF and acetone for approximately three hours at 70 °C. The $BaTiO_3$/$NiFe_2O_4$ nanomaterial was bath-sonicated for two hours at a concentration of 2 wt% in the same solvent mixture to form separate dispersions. Then, filler dispersions and PVDF solutions were magnetically stirred for a whole night to make polymer nanocomposite suspensions of PVDF/$BaTiO_3$-$NiFe_2O_4$ for electrospinning. Fig. 1 provides a schematic representation of the fabrication procedures used in this study.

2.4. Characterization techniques

Using a scanning electron microscope (Nova Nano SEM 450), we investigated the surface morphology of nanomaterials and nanocomposite fibers. A 10° to 70° X-ray diffractometer (Empyrean, Panalytical, UK) was used to analyze the structural properties. X-ray photoelectron spectrum was recorded using Kratos Axis Ultra DLD. An experimental setup was developed to study the piezoelectric characteristics. A frequency generator, an amplifier, a vibrating shaker, a resistor box, and a data collection device were some of the parts used in the setup. Samples were cut in to circular pieces of 2 cm diameter and placed on the top of the vibrating shaker under a force of 2.5 N. While the shaker imparts vibrations according to the frequency generator (50 Hz), the force applied to the fibers generated output voltage. The

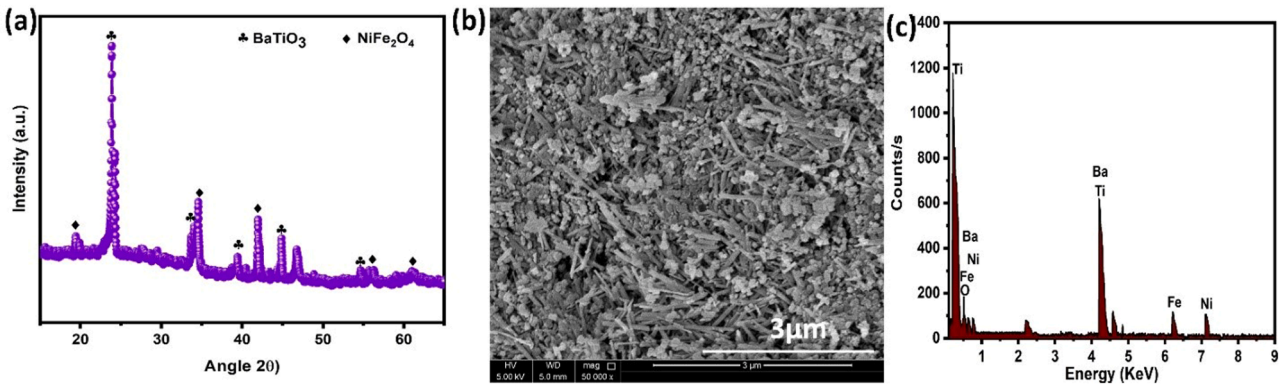

Fig. 2. (a) XRD spectra, (b) SEM image and (c) EDX spectra of $BaTiO_3$/$NiFe_2O_4$ composite.

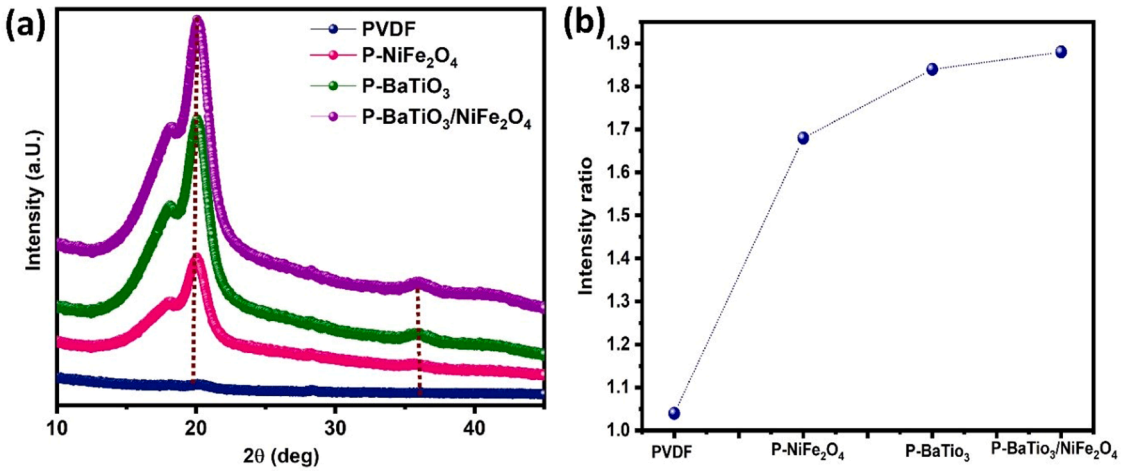

Fig. 3. (a) XRD spectra of PVDF and its nanocomposites, (b) the calculated intensity ratio for the PVDF and its nanocomposites.

software from National Instruments can be used to monitor the voltage signals made as a result. Broadband dielectric spectroscope NOVO Control Technologies, Germany (GMbH concept 40) and the universal testing machine AMETEK, Inc., Bognor Regis, UK (Lloyd 1KN LF Plus) were used to measure the samples' dielectric properties and mechanical properties, respectively.

3. Results and discussion

3.1. Structural and morphological analysis of the $BaTiO_3/NiFe_2O_4$ filler

Fig. 2a shows the powder X-ray diffraction patterns of the $BaTiO_3$/$NiFe_2O_4$ composite. The $BaTiO_3$ and $NiFe_2O_4$, have distinct peak values in the $BaTiO_3/NiFe_2O_4$ composites XRD pattern, indicating the formation of the composite structure. The $BaTiO_3$ diffraction peaks at 2 =

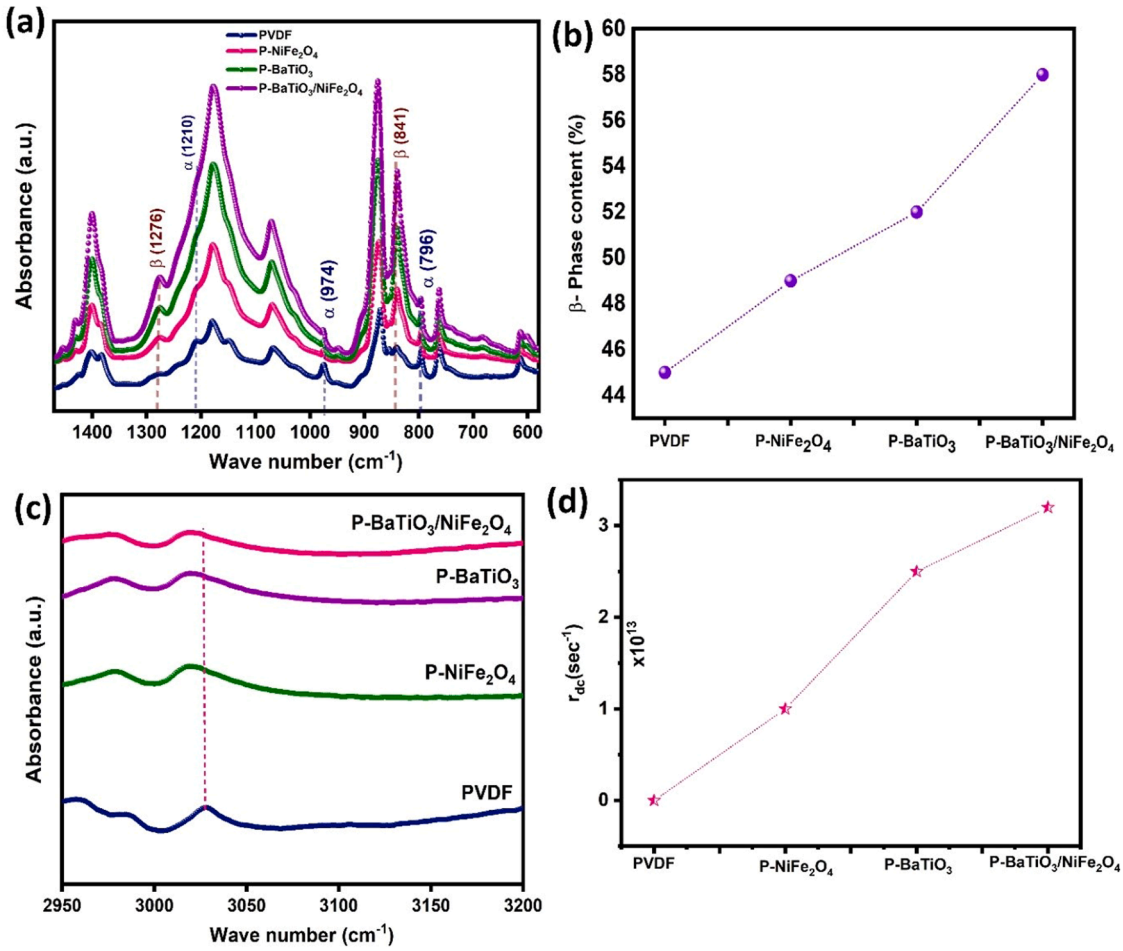

Fig. 4. (a) FTIR spectra (1600–600 cm^{-1}) (b) phase values percentage (c) FTIR spectra (2950–3200 cm^{-1}) and (d) damping coefficient variation for the PVDF and polymer nanocomposites.

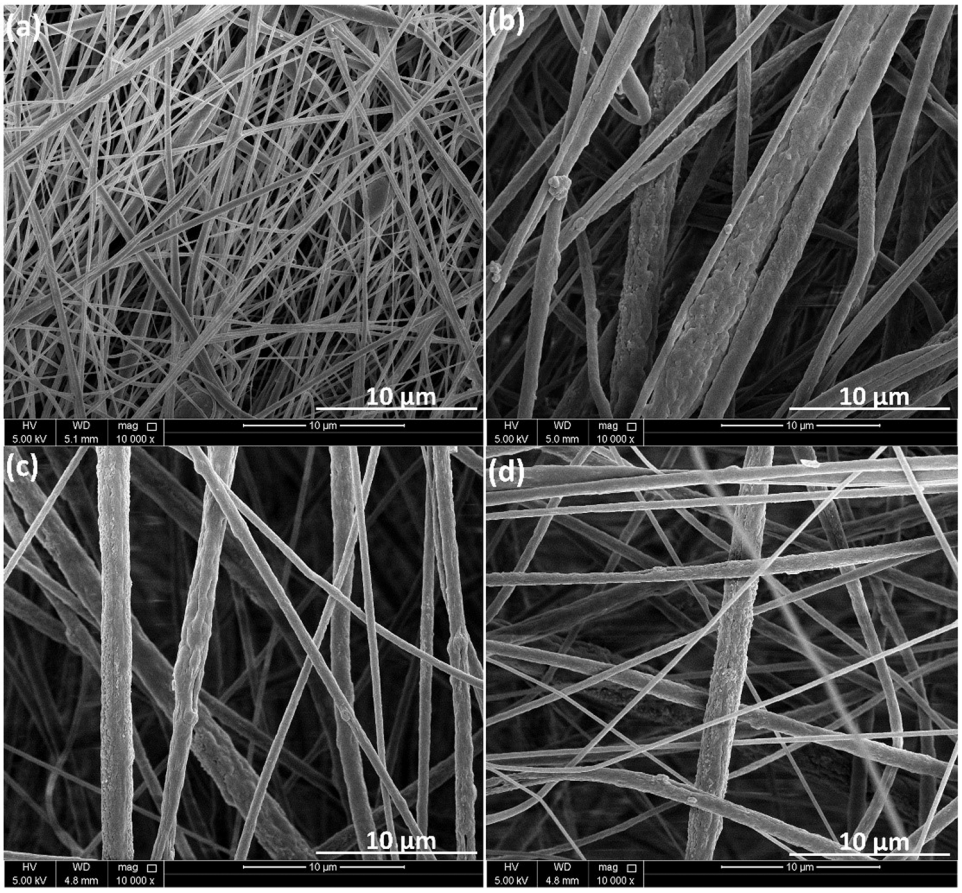

Fig. 5. Surface morphology of PVDF nanocomposites (a) PVDF, (b) P-$BaTiO_3$, (c) P-$NiFe_2O_4$, (d) P-$BaTiO_3$/$NiFe_2O_4$.

24.1°, 31.4°, 38.8°, 45.0°, and 56.1° correspond to the tetragonal $BaTiO_3$ crystallographic planes (103), (101), (111), (200), and (112/211), respectively. JCPDS 05–0626 shows these crystalline planes correspond to the tetragonal $BaTiO_3$. For the $NiFe_2O_4$ sample (JCPDS 22–1086), the crystalline planes (111), (311), (400), (511), and (533), which are found at 2 = 18.5°, 35.8°, 43.4°, 57.3°, and 63°, respectively, indicate the cubic-spinel structure of $NiFe_2O_4$. The XRD pattern demonstrated the highest purity of the composites containing $BaTiO_3$ and $NiFe_2O_4$, revealing no extra minor peaks or components in the samples. The prepared sample shows a good crystalline nature, indicating the existence of solid diffraction peaks.

Fig. 2(b, c) presents SEM images and EDX spectra of $BaTiO_3$/$NiFe_2O_4$ composites. The composite of $BaTiO_3$/$NiFe_2O_4$ is formed by $BaTiO_3$ and $NiFe_2O_4$, illustrated in Fig. 2b. The $BaTiO_3$/$NiFe_2O_4$ composite elements of Ba, Ni, Fe, Ti, and O were confirmed by the EDX analysis results shown in Fig. 2c, which showed no impurities in the sample.

3.2. Structural and morphological analysis of the electrospun nanocomposites

PVDF and its copolymers have been widely used because of the importance of the β-phase for enhancing their piezoelectricity. FTIR and XRD techniques were used to investigate the β-phase content and structural properties of PVDF and its nanocomposites, which consist of $NiFe_2O_4$, $BaTiO_3$, and $BaTiO_3$/$NiFe_2O_4$. The nucleation and crystallinity were further investigated using XRD analysis. Fig. 3(a, b) shows the findings for each nanocomposite system. The peak at 17.6 ° is associated with the α-phase and corresponds to the (100) crystal plane. The β-phases is represented with the crystal planes (110)/(200) associated with the peak at 20.5° [21]. For the PVDF composite containing the $BaTiO_3$/$NiFe_2O_4$ nanofiller, this peak gradually becomes stronger until it reaches its maximum intensity. This result suggests that the $BaTiO_3$/$NiFe_2O_4$ nanofiller also influences the XRD pattern of the composite. The increased β-phase intensity observed in these materials proves that electroactive β-phase is formed in nanocomposites containing filler.

The ratio of peak intensity values at 20.5° and 17.6°, as shown in Fig. 3b, indicates the amount of a polymer that contains the α and β-phases [22]. The pure PVDF had an average intensity ratio of approximately 1.02, which was lower than samples with $BaTiO_3$, $NiFe_2O_4$, and $BaTiO_3$/$NiFe_2O_4$ nanostructures, which had a higher intensity ratio. The results also show that the PVDF composite, containing $BaTiO_3$/$NiFe_2O_4$ nanofiller, has the highest electroactive phase composition and transformation. In addition, the filler polymer shows the highest level of interfacial interaction.

The FTIR results of the prepared nanocomposites are shown in Fig. 4 (a-d). The FTIR spectra can determine the polymer phases and crystallinity of PVDF and its nanocomposites. The -CF_2 bending and -CH_2 rocking vibrations are represented by the distinctive absorbance bands at 615, 764 cm^{-1}, 795, and 975 cm^{-1}. These bands are due to the α-phase. Fig. 4a shows that the β-phase is responsible for bands at 1433 and 1276 cm^{-1}, whereas the β and γ regions of PVDF are responsible for smaller bands at 840 cm^{-1} [23]. The values of absorbance at 840 cm^{-1} in nanocomposite films acts as a quantitative indicator of the electroactive phases presence. If $I_{wavenumber}$ is the absorbance intensity at that wavenumber and Aβ represents the regions beneath the corresponding peaks, then Fβ represents the electroactive phase content, respectively [24]. The amount of the β-phase content can be calculated using the following equations.

$$F_\beta = F_{EA}\left(\frac{A_\beta}{A_\beta + A_\gamma}\right)X100 \quad (1)$$

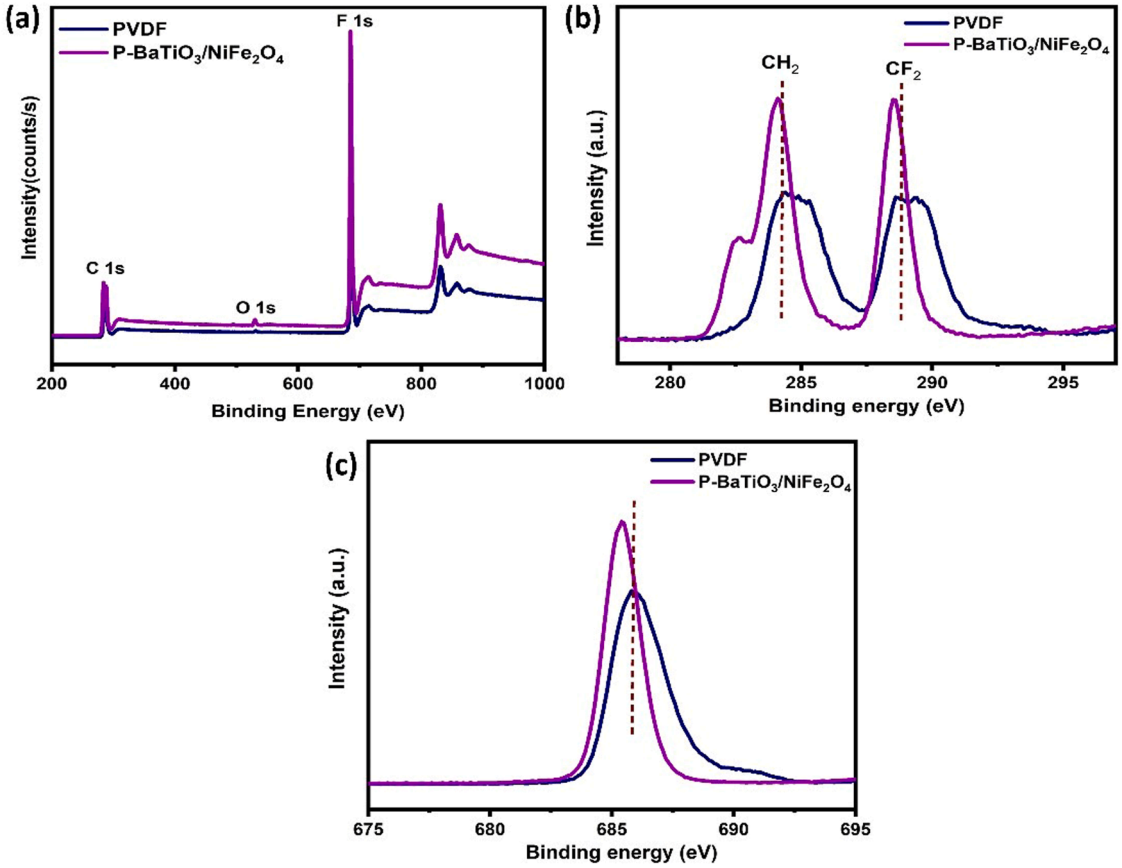

Fig. 6. (a) Survey spectra of pure PVDF and its nanocomposites samples (b, c) C 1 s and F 1 s spectrum of pure PVDF and its nanocomposites.

Fig. 4b depicts polymer nanocomposites' electroactive phase content (FEA). The nanoparticles contribute significantly to the nucleation of the electroactive phase. The electrostatic interaction between the CH_2/CF_2 dipoles and the nanoparticle surface is depicted in the FEA content. These results highlight the significance of $BaTiO_3$, $NiFe_2O_4$, and $BaTiO_3/NiFe_2O_4$ fillers in forming electroactive phases in the PVDF base polymer. It also plays a role in the transition from the lower electroactive γ-phase to the higher electroactive β-phase [25]. The composite comprising $BaTiO_3/NiFe_2O_4$ has the highest crystallinity, and the FTIR results agree with the XRD results.

Electrostatic interactions are responsible for this, as indicated by the $-CH_2-/-CF_2-$ dipoles in PVDF and the surface charge in $BaTiO_3/NiFe_2O_4$. Through aggregating all locally ordered trans-conformations, the surface charges in the nanofiller interact with the $-CF_2-$ dipoles of the PVDF segments in the nanocomposite to stabilize the polar γ-phase. The FTIR spectrum between 3200 and 2950 cm^{-1} shows the symmetric νs ($-CH_2-$) and asymmetric vas ($-CH_2-$) stretching (Fig. 4c). The bands in this area show the occur interface interactions between the PVDF matrix and the $BaTiO_3/NiFe_2O_4$ filler. The occurrence of interfacial contacts among the PVDF and the $BaTiO_3/NiFe_2O_4$ filler in the nanocomposites is seen in Fig. 4c by the shifting of the $v_{as}(-CH_2-)$ and v_{as} ($-CH_2-$) vibrational bands in the nanocomposite to a lower frequency range when compared to pure PVDF. As the filler loading increases, the peak location gradually shifts due to the damping oscillations of the $-CH_2-$ dipoles. Due to electrostatic interactions between the dipoles and a charge on the surface of the $BaTiO_3/NiFe_2O_4$ filler, the effective mass of the $-CH_2-$ dipoles in PVDF increased. The following formula can calculate the damping coefficient (r_{dc}).

$$r_{dc} = 4\pi c \quad \left(\vartheta^2_{Polymer} - \vartheta^2_{Nanocomposite}\right)^{0.5} \tag{2}$$

where υ is the wavenumber of the free vibration caused by the presence of $-CH_2$ and C is the speed of light. The damped harmonic oscillations of $-CH_2$ dipoles are associated to the rdc in addition to the polymer-filler electrostatic interaction [26]. Fig. 4d illustrates that the damping coefficient values increase as the filler concentration increases. This may occur due to the concentration of $BaTiO_3/NiFe_2O_4$ filler within the PVDF matrix percolating. The presence of charge in the $BaTiO_3/NiFe_2O_4$ filler causes the $-CH_2-$ dipoles to interact electrostatically, indicating a direct correlation between the attenuation coefficient and the nature of the electroactive phase development. Due to the ion-dipole interaction caused by the formation of the electroactive phase, the PVDF chain attempted to attract some components while repelling others in the nanocomposite.

The morphology and average fiber diameter of polymer nanocomposite fibers were studied. Fig. 5 shows SEM images of PVDF and composite fibers. Fig. 5a shows SEM images of defect-free fibers (no beads) because the PVDF solution used for electrospinning was at the optimum concentration. The fiber morphology and diameter show a minor variance when the nanomaterials are incorporated into the PVDF matrix (Fig. 5(b-d)). The concentration of the polymer solution and the applied voltage cause the nanocomposite solutions' Taylor cone regions to fluctuate, influencing the mass flow of the downstream jet. As a result of the previously mentioned, the distribution of charges on the jet surface gradually changes, which influences variations in fiber diameter. When the applied voltage is changed, there is an inconsistency between the flow of solution to the needle tip and the needles withdrawal with the help of the electric field. The increased fiber diameter could be attributed to the nanocomposites' enhanced viscosity and networking effect, contributing to the uniform filler distribution. The composite samples showed minor variations in fiber diameter because of the PVDF polymers uniform proportions of filler dispersion.

XPS was utilized to further investigate the interfacial interaction

Table 1
The nanocomposites mechanical properties.

Sample	Tensile strength (MPa)	Young's modulus (MPa)	Elongation at break (%)
PVDF	19.23 ± 1.2	62.31±1.2	12.31± 2.1
P-$NiFe_2O_4$	22.64 ± 3.1	72.31± 9.25	10.21±1.2
P-$BaTiO_3$	29.34 ± 1.4	84.31 ± 3.5	8.32 ± 0.81
P-$BaTiO_3$/ $NiFe_2O_4$	39.04 ± 1.52	95.88 ± 7.25	6.01 ± 1.01

between the polymer and filler [27]. Fig. 6(a-c) shows the XPS images of pure PVDF and P-$BaTiO_3$/$NiFe_2O_4$ composite fibers. Strong peaks that correspond to the fluorine and carbon atoms in the PVDF skeleton appeared at 282–288 and 688 eV, respectively. The C 1 s spectrum of PVDF and its nanocomposites are shown in Fig. 6b. The strong peak at 282 and 288 eV correspond to the –CH_2 and –CF_2 groups of PVDF [28].

The C1 XPS spectra of P-$BaTiO_3$/$NiFe_2O_4$ also contains these carbons, with a clear shift to the low energy region. On the other hand, the XPS spectra of F 1 s show the peaks at 687.6 and 686.9 eV for pure PVDF and P-$BaTiO_3$/$NiFe_2O_4$, respectively (see Fig. 6c). The shifting of C and F peaks for P-$BaTiO_3$/$NiFe_2O_4$ sample is due to the occurrence of more interactions between dipole ($C^{\delta+}$-$F^{\delta-}$) of PVDF chain and $BaTiO_3$/$NiFe_2O_4$ nanofiller [29].

Table 1 shows the mechanical properties of the composites. It is vital to examine the mechanical properties of composite materials before using them in self-sufficient systems. In this case, the addition of nanoparticles significantly increases the tensile strength. The increase in both Young's modulus and tensile strength values is explained by the increased crosslink density attributed to the incorporation of nanofillers. The elongation at break decreased when nanofillers were added, while the tensile strength and Young's modulus increased. It is suggested that the lower elongation at break is due to increased crosslinks and decreased polymer chain mobility. This agrees with the XRD analysis and the SEM morphological changes. These all indicate that adding nanofiller influences the polymer chains' mobility and generates links, improving mechanical energy performance.

3.3. Dielectric properties of the nanocomposites

To evaluate PVDFs and their nanocomposites frequency-dependent dielectric properties, the dielectric constant and loss figures at various frequencies are investigated (Fig. 7(a-c)). Compared to the pure PVDF, the dielectric constant values of $BaTiO_3$, $NiFe_2O_4$, and $BaTiO_3$/$NiFe_2O_4$ incorporated PVDF composite fiber were increased (Fig. 7a), which can be explained by the fillers polar nature [30]. Additionally, it is observed that greater values are obtained when the addition of $BaTiO_3$/$NiFe_2O_4$ nanofiller. Compared to the polar phase fraction obtained from FTIR and XRD data, PVDF/$BaTiO_3$-$NiFe_2O_4$ has the highest dielectric permittivity. It showed that nanofiller significantly impacted composite homogeneity and dielectric permittivity. This was attributed to the strong interaction between the functional group of the nanofiller and the PVDF matrix. This showed the enhanced interfacial contact between the polymer and nanofiller [31]. As Huang et al. [24] reported, a coated surface layer on nanoparticles produced a strong nanoparticle/matrix interaction. Two key elements are responsible for the improvement in dielectric properties. The first is the interfacial polarization effect of Maxwell-Wagner-Sillars (MWS), which occurs by charge accumulation at interfaces in heterogeneous media composed of phases with varying conductivities and permittivity [32]. When the interparticle distance

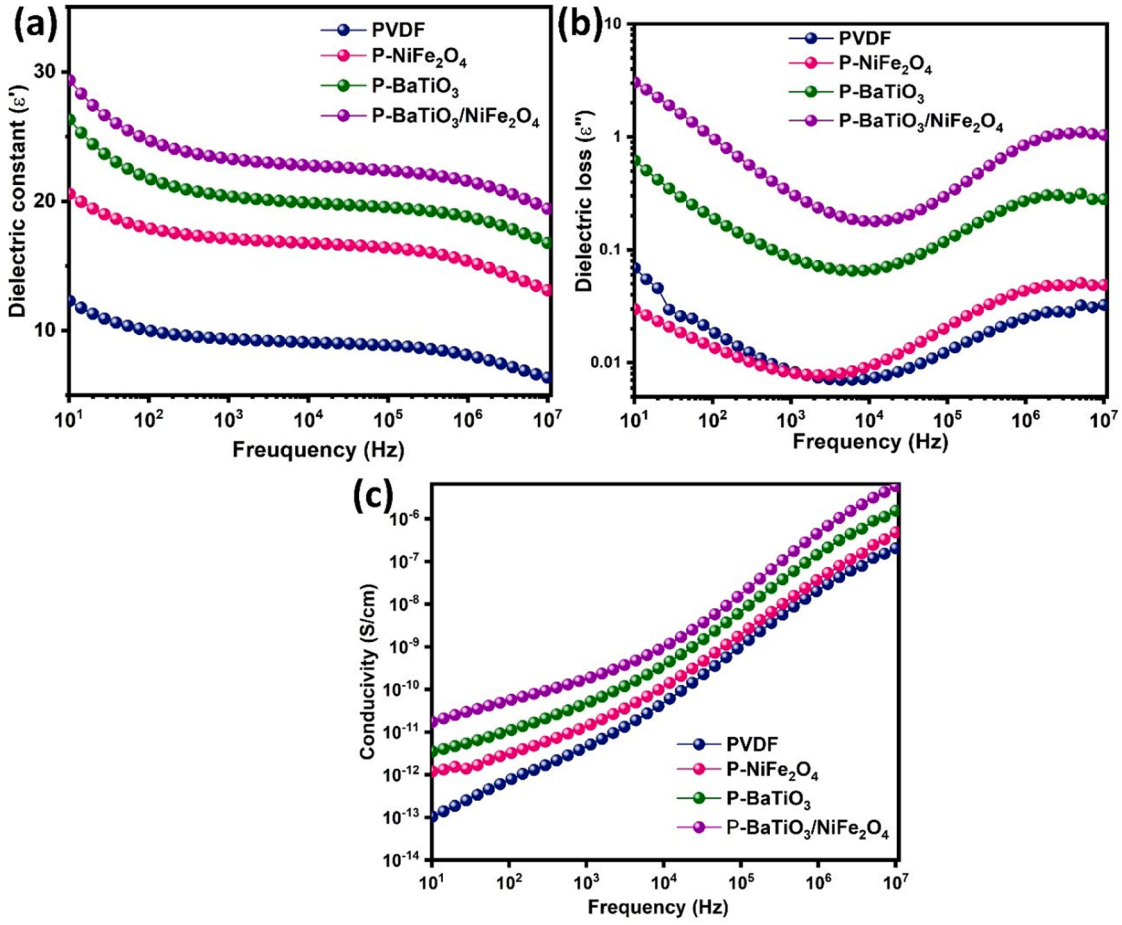

Fig. 7. Frequency dependence of (a) dielectric constant (ε') (b) dielectric loss (ε") and (c) conductivity spectra of the pure PVDF and its nanocomposites fibers.

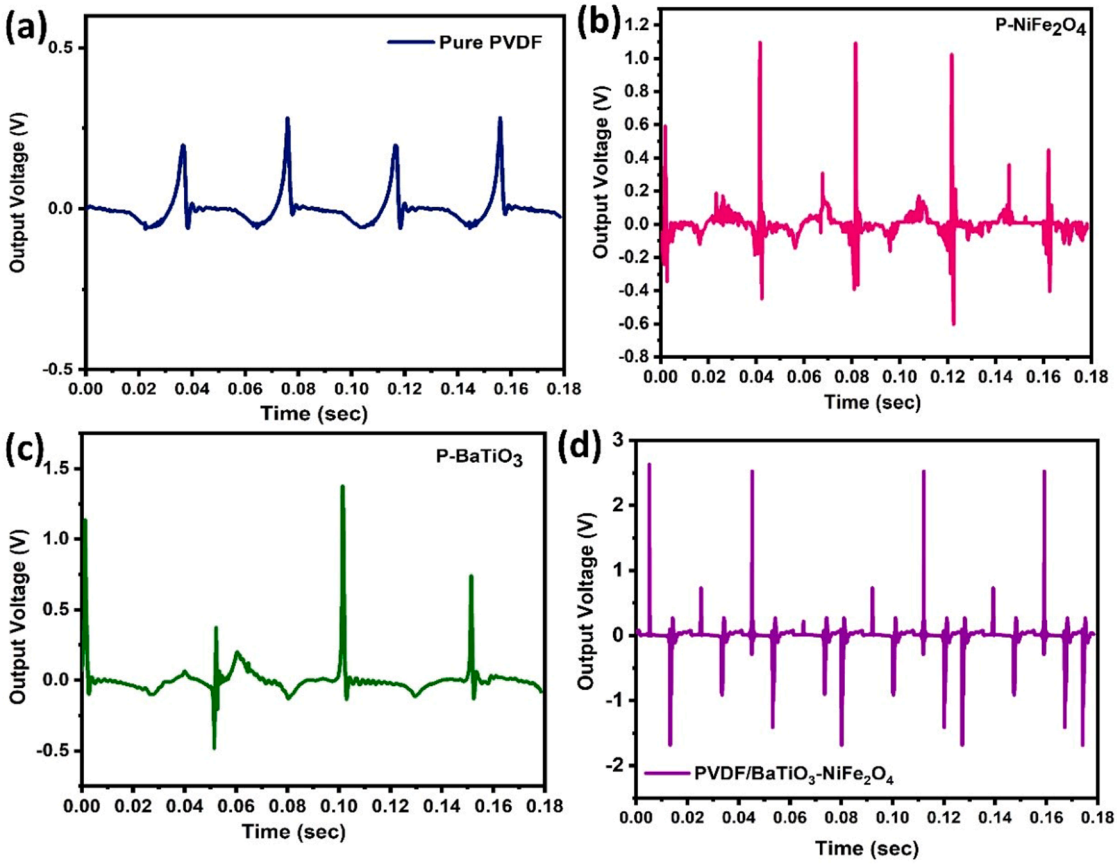

Fig. 8. The electrical output performance of the PENG under 2 N load, (a) pure PVDF, (b) P-$NiFe_2O_4$, (c) P-$BaTiO_3$, and (d) P/$BaTiO_3$-$NiFe_2O_4$.

reduces with the addition of nanofiller, the number of NPs and their interfacial area increase. This improves the coupling between adjacent grains and the average polarization of the NPs, significantly increasing the dielectric characteristics of nanocomposite films. The electroactive phase composition of the polymer nanocomposite samples could be the main reason for their observed dielectric properties. However, the samples' dielectric loss values were lower (Fig. 7b), which is usually preferred for energy storage applications [33]. As seen in Fig. 7b, the loss values of the composites are significantly higher than those of the pure PVDF at low frequencies as the incorporation of nanofillers. Because of their conductive nature as well as the loss factor, the dielectric loss increases for the composite samples, but it is less than that of composites containing conductive fillers such carbon black, carbon fiber, carbon nanotubes, etc., [34]. The conduction process of ions and dipoles may be responsible for of the significant dielectric loss for the P-$BaTiO_3$/$NiFe_2O_4$ composites at low frequencies. At low frequencies, the loss is significantly higher and induces relaxations due to interfacial polarization and Debye losses. The loss decreases with increasing frequency [35]. For both pure PVDF and its nanocomposites, the composition of the dielectric loss factors shifting with frequency is quite similar with previous research [36,37]. Due to dipole polarization, the dielectric loss factor-frequency curve of PVDF typically has a peak at roughly 10^6–10^7 Hz (*fp*). Three is sufficient time in the low-frequency band for the dipoles to orient under the AC electrical field. On the other hand, dipoles cannot move at a high frequency in the short period of time provided. Because there is constant friction generating a lot of heat dissipation, when the frequency is close to *fp*, the dipoles can move to keep up with the charge of the AC electrical field and achieve the highest dielectric loss factor [29].

Interface charge polarization and related electric dipole polarization inside the composites in applied alternating field could account for an increase in dielectric constant and loss tangent with the addition of filler particles [38,39]. Due to the buildup of electric charges at the interface boundaries and the development of significant dipoles on ceramic particles or clusters, this phenomena occurs in heterogeneous systems such as ceramic-polymer composites. It is generally accepted that the high volume fraction of interfaces in nanocomposites increases the possibility of interfacial polarization [40].

The variation of the conductivity as a function of frequency for pure PVDF, P-$NiFe_2O_4$, P-$BaTiO_3$ and P-$BaTiO_3$/$NiFe_2O_4$ is shown in Fig. 7c. The conductivity values for PVDF and its composites give results that are comparable to other composites [41]. It is evident that the interfacial polarization effect causes the conductivity of PVDF and its composites to increase with frequency. A nanocomposite system consists of an insulating polymer matrix and nanofillers with relatively high conductivity values. This charge difference induces surface polarization and charge accumulation at the filler-polymer interfaces. This interfacial polarization happens at low frequency region where the conducting nanofillers act as small capacitors and this phenomenon is referred to as Maxwell-Wagner-Sillars effect [42,43].

3.4. *Piezoelectric properties*

In addition to the previous discussion, the addition of nanofillers increases crosslink formation and introduces interfacial contacts between the layers of $BaTiO_3$/$NiFe_2O_4$ and PVDF chains. The XRD, FT-IR, SEM, and dielectric data observations were used as the basis for this evaluation. The effectiveness of the PVDF/$BaTiO_3$-$NiFe_2O_4$ nanocomposite films to capture mechanical energy was investigated by fabricating an electrode composite electrode (ECE) stack, where the electrode was an aluminium foil. The piezoelectric responses of all the nanocomposites were examined using the methodology explained in the

Table 2
Values of the resultant power density for pure PVDF, P-$BaTiO_3$, P-$NiFe_2O_4$, and P-$BaTiO_3$/$NiFe_2O_4$ nanocomposites.

Sample	Power density (μW cm^{-2})
PVDF	0.016
P-$NiFe_2O_4$	0.189
P-$BaTiO_3$	0.195
P-$BaTiO_3$/$NiFe_2O_4$	1.095

previous work [44]. Mechanical forces were applied to the samples using a shaker, which increased the frequency of vibration. The piezoelectric nanogenerators showed a range of output voltages by their compositions, which are shown in Fig. 8(a-d) PVDF/$BaTiO_3$-$NiFe_2O_4$ nanocomposite films demonstrated a maximum output voltage of 4.1 V. This was more than eight times larger than the pure polymer. In addition, the $BaTiO_3$ and $NiFe_2O_4$ nanomaterials show higher output voltage compared to pure PVDF at the same filler concentration. The output voltage performance for all samples was evaluated and compared in Fig. 8. Filler loading increases the output voltage. The crystal structures' response to applied mechanical pressure generally influences output voltage generation [45]. When materials are subjected to pressure, the electric dipoles align consistently, producing a high electric field.

Following the equation is the instantaneous power density,

$$\rho = \frac{V^2}{RA}$$

where A is the effective electrode area, R is the load, and V is the voltage. The output densities of each composite are displayed in Table 2 (under a load resistance of 1 MΩ). The influence of the filler particle on altering the electroactive phases of PVDF and the increase in the β-phase content of PVDF in the presence of $BaTiO_3$/$NiFe_2O_4$. Pusty et al. [46], state that the processing technique, filler addition, concentration of the filler, and β-crystalline phase composition were responsible for PVDFs enhanced piezoelectric properties. The samples XRD, SEM, and FTIR results guarantee the significance of the crystalline phase composition and filler addition. It has been found that $BaTiO_3$/$NiFe_2O_4$ nanoparticles are essential for enhancing output performance.

Fig. 9(a-c). shows the Nyquist plot of the devices obtained using the complex impedance response at an input frequency range of 0.1 Hz to 100 kHz. A semi-circular arc-shaped pattern in dielectric spectroscopy indicates the presence of an RC circuit [47]. For every device, the time constant (τ_{RC}) was determined using the critical frequency $\left(\tau_{RC} = \frac{1}{2\pi f_c}\right)$, which was obtained from the arcs marked with the corresponding resonant frequencies, *fc* (Fig. 9). The time constant (τ_{RC}) values were observed to increase with the addition filler particles.

For pure PVDF, P-$NiFe_2O_4$, P-$BaTiO_3$ and P-$BaTiO_3$/$NiFe_2O_4$ composites with 0.03 ms, 0.12 ms, 0.28 ms and 1.28 ms time constants. According to reports, the suppression of surface states in samples of PVDF with filler reduced the free carrier density, which in turn reduced the rate of internal polarization field screening in PVDF. The time constant (τ_{RC}) in PVDF indicates an increase in the duration of the polarization field, leading to a higher value of the potential difference across the PVDF. As a result, the composite samples' observed peak-to-peak voltage was higher than that of the pure PVDF. Hence, the relationship between the device time constant (τ_{RC}) and the voltage from peak to peak elucidates the internal polarization field screening phenomenon that results from PVDF surface-state injected free carriers [48]. This can be further explained with a model of a lossy capacitor [49] (Fig. 10). As a

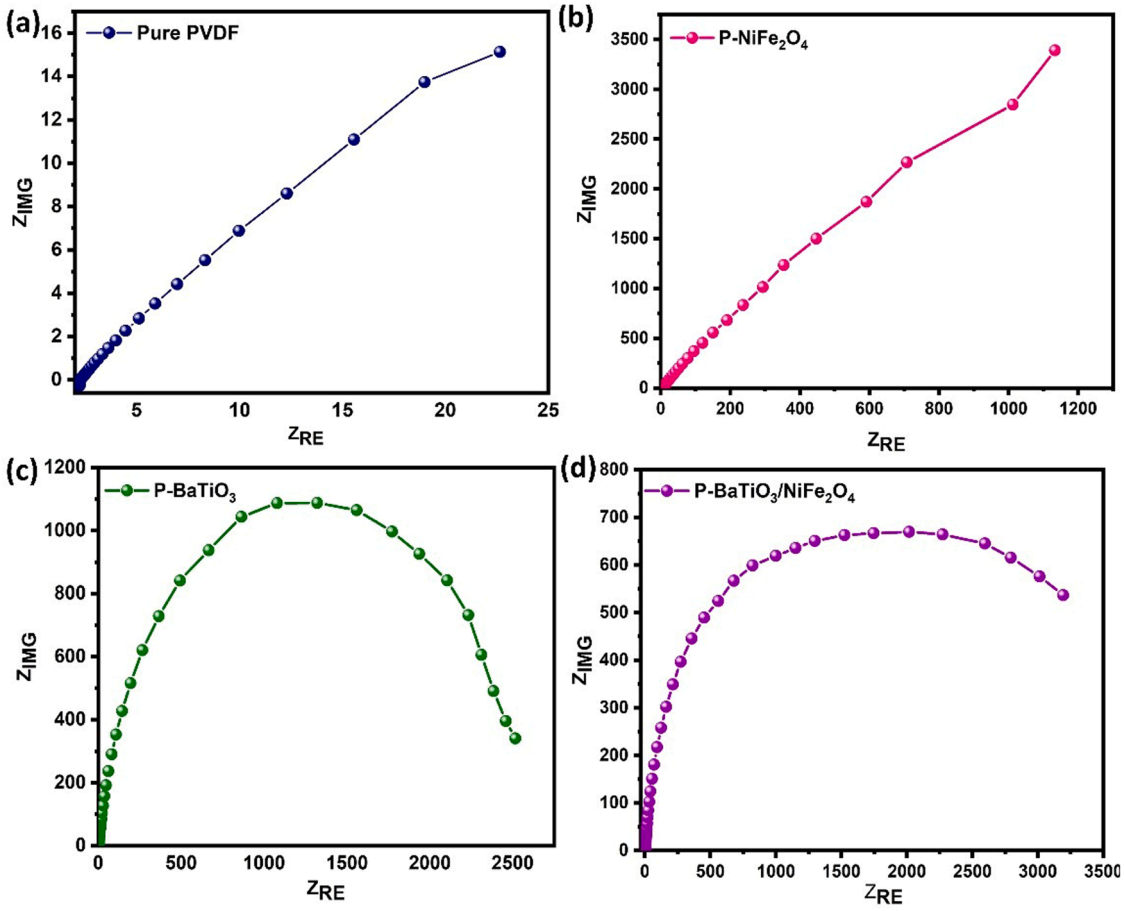

Fig. 9. Nyquist plots of (a) pure PVDF, (b) P-$NiFe_2O_4$, (c) P-$BaTiO_3$ and (d) P-$BaTiO_3$/$NiFe_2O_4$.

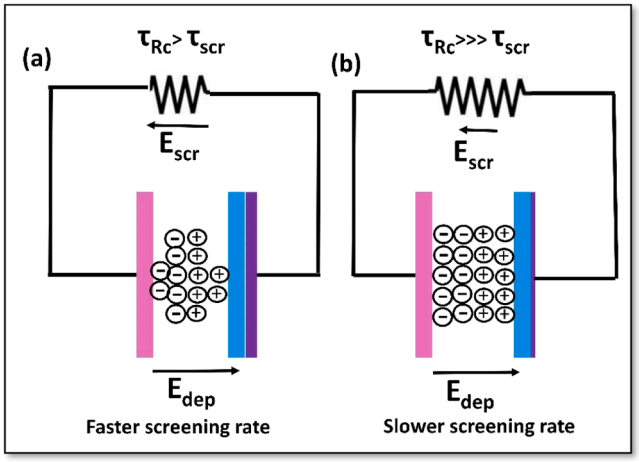

Fig. 10. (a, b) Piezoelectric source modeling: the internal impedance of nanofibers is modeled as a resistor, and they are represented as a parallel plate capacitor. The increase in charge storage between the parallel plates is caused by the decrease in screening of the depolarization field (E_{dep}), which is represented as a reduced screening field (E_{scr}). The net retention of polarized charges is represented as stored charges.

dielectric material, piezoelectric PVDF can be represented as a leaking resistance in parallel with a lossless capacitor. The conductivity of PVDF is represented by the leakage resistance, which varies according to the carrier concentration generated by the surface state. The dipole moment in PVDF produced by the piezoelectric strain causes charge separation, which results in the development of the depolarization field (E_{dep}) [50]. The internal carrier screening is denoted by a screening field (E_{scr}) positioned opposite to E_{dep}. When compared to filler-incorporated PVDF (Fig. 10b), pure PVDF tends to screen the stored polarization charges more quickly, which is facilitated by its reduced leakage resistance (Fig. 10a). Therefore, as confirmed by the time constant (τ_{RC}) results, the duration of retention of polarized charges of the composites samples ((τ_{RC} = 0.12 ms, 0.28 ms and 1.28 ms) was higher than the pure PVDF sample (τ_{RC} = 0.03ms).

4. Conclusion

In conclusion, the electrospinning technology was used to fabricate the PVDF/$BaTiO_3$-$NiFe_2O_4$ based electrospun fibers for application in piezoelectric energy harvesting. The fabricated composite fibers were found to increase the formation of the β-phase, as revealed by functional group and structural studies. The composite nanofibers of PVDF/$BaTiO_3$-$NiFe_2O_4$ showed a maximum β-phase of 58%. This was more appropriate to achieve high piezoelectricity in PVDF composite materials. When $BaTiO_3$/$NiFe_2O_4$ nanofiller was added, dielectric measurements revealed an enhanced dielectric constant for the PVDF/$BaTiO_3$-$NiFe_2O_4$ composite fiber samples, a maximum dielectric constant of 29 was achieved. It was found that the $BaTiO_3$/$NiFe_2O_4$ composite nanofibers exhibit an increase in piezoelectric output voltage. A maximum peak-to-peak output voltage of 4.1 V was generated using a fabricated piezoelectric nanogenerator with an applied force of 2 N. The nanogenerator demonstrated a low dielectric loss and high dielectric constant, making it appropriate for energy storage systems. These findings indicate that an energy harvesting system can effectively use the flexible piezoelectric nanogenerator.

CRediT authorship contribution statement

Hemalatha Parangusan: Writing – original draft, Methodology, Formal analysis, Data curation, Conceptualization. **K. Karuppasamy**: Writing – review & editing, Validation, Investigation. **Jolly Bhadra**: Writing – review & editing, Project administration, Funding acquisition.

Declaration of Competing Interest

The authors declare that they have no known competing financial interests or personal relationships that could have appeared to influence the work reported in this paper.

Data Availability

Data will be made available on request.

Acknowledgment

This study was supported by UREP 28–190–2–046 from the Qatar National Research Fund. The findings herein are solely the responsibility of the authors. The authors are also very grateful to the Center for Advanced Materials (CAM), Qatar University for the inclusive support. This works characterizations were carried out at Qatar University Central Laboratories Unit (CLU) for morphological analysis and the Gas Processing Center (GPC) for XPS analysis. Open Access funding provided by the Qatar National Library (QNL).

References

[1] K.I. Park, M. Lee, Y. Liu, S. Moon, G.T. Hwang, G. Zhu, J.E. Kim, S.O. Kim, D. K. Kim, Z.L. Wang, Flexible nanocomposite generator made of BaTiO3 nanoparticles and graphitic carbons, Adv. Mater. 24 (2012) 2999–3004.
[2] G.J. Aubrecht, I. Aubrecht, Energy: physical, environmental, and social impact, Pearson Prentice Hall Upper Saddle River, NJ, 2006.
[3] S.R. Anton, H.A. Sodano, A review of power harvesting using piezoelectric materials (2003–2006), Smart Mater. Struct. 16 (2007) R1.
[4] H.A. Sodano, G. Park, D. Inman, Estimation of electric charge output for piezoelectric energy harvesting, Strain 40 (2004) 49–58.
[5] F. Wang, Y.-W. Mai, D. Wang, R. Ding, W. Shi, High quality barium titanate nanofibers for flexible piezoelectric device applications, Sens. Actuators A: Phys. 233 (2015) 195–201.
[6] Z.L. Wang, Zinc oxide nanostructures: growth, properties and applications, J. Phys. Condens. Matter 16 (2004) R829.
[7] H. Parangusan, J. Bhadra, Z. Ahmad, K. Karuppasamy, S. Mallick, F. Touati, N. Al-Thani, Hierarchical BaTiO3/NiFe2O4 nanocomposite as an efficacious photoanode for photoelectrochemical water splitting, Ceram. Int. 48 (2022) 29136–29143.
[8] H. Parangusan, J. Bhadra, K. Karuppasamy, T. Maiyalagan, Z. Ahmad, N. Al-Thani, Engineering the structural, optical and photoelectrochemical properties of BaTiO3-CoFe2O4 nanocomposite for photoelectrochemical water splitting, Electrochim. Acta 464 (2023) 142849.
[9] S. Egusa, Z. Wang, N. Chocat, Z. Ruff, A. Stolyarov, D. Shemuly, F. Sorin, P. Rakich, J. Joannopoulos, Y. Fink, Multimaterial piezoelectric fibres, Nat. Mater. 9 (2010) 643–648.
[10] K. Karuppasamy, K. Prasanna, D. Kim, Y.H. Kang, H.W. Rhee, Headway in rhodanide anion based ternary gel polymer electrolytes (TILGPEs) for applications in rechargeable lithium ion batteries: an efficient route to achieve high electrochemical and cycling performances, RSC Adv. 7 (2017) 19211–19222.
[11] I. Chinya, A. Pal, S. Sen, Polyglycolated zinc ferrite incorporated poly (vinylidene fluoride)(PVDF) composites with enhanced piezoelectric response, J. Alloy. Compd. 722 (2017) 829–838.
[12] J. Theerthagiri, K. Karuppasamy, A. Min, D. Govindarajan, M.L.A. Kumari, G. Muthusamy, S. Kheawhom, H.-S. Kim, M.Y. Choi, Unraveling the fundamentals of pulsed laser-assisted synthesis of nanomaterials in liquids: applications in energy and the environment, Appl. Phys. Rev. 9 (2022).
[13] H.J. Ye, W.Z. Shao, L. Zhen, Crystallization kinetics and phase transformation of poly (vinylidene fluoride) films incorporated with functionalized BaTiO3 nanoparticles, J. Appl. Polym. Sci. 129 (2013) 2940–2949.
[14] T.U. Patro, M.V. Mhalgi, D. Khakhar, A. Misra, Studies on poly (vinylidene fluoride)–clay nanocomposites: effect of different clay modifiers, Polymer 49 (2008) 3486–3499.
[15] B. Dutta, E. Kar, N. Bose, S. Mukherjee, Significant enhancement of the electroactive β-phase of PVDF by incorporating hydrothermally synthesized copper oxide nanoparticles, RSC Adv. 5 (2015) 105422–105434.
[16] K. Karuppasamy, B. Sharma, D. Vikraman, E.-B. Jo, P. Sivakumar, H.-S. Kim, Switchable p-n gas response for 3D-hierarchical NiFe2O4 porous microspheres for highly selective and sensitive toluene gas sensors, J. Alloy. Compd. 886 (2021) 161281.
[17] D. Vikraman, H. Liu, S. Hussain, S.H.A. Jaffery, K. Karuppasamy, E.-B. Jo, Z. Abbas, J. Jung, J. Kang, H.-S. Kim, Impact of molybdenum dichalcogenides on the active and hole-transport layers for perovskite solar cells, X-Ray Detect. Photo Small 18 (2022) 2104216.

[18] E.S. Cozza, O. Monticelli, E. Marsano, P. Cebe, On the electrospinning of PVDF: Influence of the experimental conditions on the nanofiber properties, Polym. Int. 62 (2013) 41–48.
[19] G. Zhong, L. Zhang, R. Su, K. Wang, H. Fong, L. Zhu, Understanding polymorphism formation in electrospun fibers of immiscible poly (vinylidene fluoride) blends, Polymer 52 (2011) 2228–2237.
[20] V. Sencadas, P. Martins, A. Pitães, M. Benelmekki, J.L. Gomez Ribelles, S. Lanceros-Mendez, Influence of ferrite nanoparticle type and content on the crystallization kinetics and electroactive phase nucleation of poly (vinylidene fluoride), Langmuir 27 (2011) 7241–7249.
[21] L. Huang, C. Lu, F. Wang, L. Wang, Preparation of PVDF/graphene ferroelectric composite films by in situ reduction with hydrobromic acids and their properties, Rsc Adv. 4 (2014) 45220–45229.
[22] P. Xu, W. Fu, Z. Cui, Y. Ding, Synergistic promotion of polar phase crystallization of PVDF by ionic liquid with PEG segment, Appl. Surf. Sci. 444 (2018) 480–484.
[23] P. Martins, A. Lopes, S. Lanceros-Mendez, Electroactive phases of poly (vinylidene fluoride): determination, processing and applications, Prog. Polym. Sci. 39 (2014) 683–706.
[24] H. Zhu, S. Yamamoto, J. Matsui, T. Miyashita, M. Mitsuishi, Ferroelectricity of poly (vinylidene fluoride) homopolymer Langmuir–Blodgett nanofilms, J. Mater. Chem. C. 2 (2014) 6727–6731.
[25] A.S. ELmezayyen, F.M. Reicha, I.M. El-Sherbiny, J. Zheng, C. Xu, Significantly enhanced electroactive β phase crystallization and UV-shielding properties in PVDF nanocomposites flexible films through loading of ATO nanoparticles: Synthesis and formation mechanism, Eur. Polym. J. 90 (2017) 195–208.
[26] S.K. Karan, D. Mandal, B.B. Khatua, Self-powered flexible Fe-doped RGO/PVDF nanocomposite: an excellent material for a piezoelectric energy harvester, Nanoscale 7 (2015) 10655–10666.
[27] D. Ponnamma, M.A.A. Al-Maadeed, 3D architectures of titania nanotubes and graphene with efficient nanosynergy for supercapacitors, Mater. Des. 117 (2017) 203–212.
[28] N. Senthilkumar, K.J. Babu, G. Gnana, kumar, A.R. Kim, D.J. Yoo, Flexible electrospun PVdF-HFP/Ni/Co membranes for efficient and highly selective enzyme free glucose detection, Ind. Eng. Chem. Res. 53 (2014) 10347–10357.
[29] F.-A. He, K. Lin, D.-L. Shi, H.-J. Wu, H.-K. Huang, J.-J. Chen, F. Chen, K.-H. Lam, Preparation of organosilicate/PVDF composites with enhanced piezoelectricity and pyroelectricity by stretching, Compos. Sci. Technol. 137 (2016) 138–147.
[30] L. Xie, X. Huang, K. Yang, S. Li, P. Jiang, Grafting to" route to PVDF-HFP-GMA/BaTiO 3 nanocomposites with high dielectric constant and high thermal conductivity for energy storage and thermal management applications, J. Mater. Chem. A 2 (2014) 5244–5251.
[31] D. Ponnamma, O. Aljarod, H. Parangusan, M.A.A. Al-Maadeed, Electrospun nanofibers of PVDF-HFP composites containing magnetic nickel ferrite for energy harvesting application, Mater. Chem. Phys. 239 (2020) 122257.
[32] Y. Li, X. Huang, Z. Hu, P. Jiang, S. Li, T. Tanaka, Large dielectric constant and high thermal conductivity in poly (vinylidene fluoride)/barium titanate/silicon carbide three-phase nanocomposites, ACS Appl. Mater. Interfaces 3 (2011) 4396–4403.
[33] K. Deshmukh, M.B. Ahamed, K.K. Sadasivuni, D. Ponnamma, M.A.A. AlMaadeed, R.R. Deshmukh, S.K. Pasha, A.R. Polu, K. Chidambaram, Fumed SiO2 nanoparticle reinforced biopolymer blend nanocomposites with high dielectric constant and low dielectric loss for flexible organic electronics, J. Appl. Polym. Sci. 134 (2017).
[34] M. Rahaman, T.K. Chaki, D. Khastgir, Polyaniline/ethylene vinyl acetate composites as dielectric sensor, Polym. Eng. Sci. 54 (2014) 1632–1639.
[35] T. Zhou, J.-W. Zha, R.-Y. Cui, B.-H. Fan, J.-K. Yuan, Z.-M. Dang, Improving dielectric properties of BaTiO3/ferroelectric polymer composites by employing surface hydroxylated BaTiO3 nanoparticles, ACS Appl. Mater. Interfaces 3 (2011) 2184–2188.
[36] A. Hartono, D. Darwin, R. Ramli, S. Satira, M. Djamal, H. Herman, Electric Field Poling 2G V/m to Improve Piezoelectricity of PVDF Thin Film. AIP Conference Proceedings, AIP Publishing, 2016.
[37] L. Zhang, S. Yuan, S. Chen, D. Wang, B.-Z. Han, Z.-M. Dang, Preparation and dielectric properties of core–shell structured Ag@ polydopamine/poly (vinylidene fluoride) composites, Compos. Sci. Technol. 110 (2015) 126–131.
[38] H.T. Vo, F.G. Shi, Towards model-based engineering of optoelectronic packaging materials: dielectric constant modeling, Microelectron. J. 33 (2002) 409–415.
[39] G. Psarras, E. Manolakaki, G. Tsangaris, Electrical relaxations in polymeric particulate composites of epoxy resin and metal particles, Compos. Part A Appl. Sci. Manuf. 33 (2002) 375–384.
[40] A. Choudhury, Dielectric and piezoelectric properties of polyetherimide/BaTiO3 nanocomposites, Mater. Chem. Phys. 121 (2010) 280–285.
[41] D. Ponnamma, A. Erturk, H. Parangusan, K. Deshmukh, M.B. Ahamed, M. Al Ali Al-Maadeed, Stretchable quaternary phasic PVDF-HFP nanocomposite films containing graphene-titania-SrTiO 3 for mechanical energy harvesting, Emergent Mater. 1 (2018) 55–65.
[42] K. Deshmukh, M.B. Ahamed, K.K. Sadasivuni, D. Ponnamma, M.A.-A. AlMaadeed, S.K. Pasha, R.R. Deshmukh, K. Chidambaram, Graphene oxide reinforced poly (4-styrenesulfonic acid)/polyvinyl alcohol blend composites with enhanced dielectric properties for portable and flexible electronics, Mater. Chem. Phys. 186 (2017) 188–201.
[43] K. Deshmukh, M.B. Ahamed, K.K. Sadasivuni, D. Ponnamma, R.R. Deshmukh, S. K. Pasha, M.A.-A. AlMaadeed, K. Chidambaram, Graphene oxide reinforced polyvinyl alcohol/polyethylene glycol blend composites as high-performance dielectric material, J. Polym. Res. 23 (2016) 1–13.
[44] H. Parangusan, D. Ponnamma, M. Al Ali Almaadeed, Flexible tri-layer piezoelectric nanogenerator based on PVDF-HFP/Ni-doped zno nanocomposites, RSC Adv. 7 (79) (2017) 50156–50165.
[45] A. Sultana, M.M. Alam, S. Garain, T.K. Sinha, T.R. Middya, D. Mandal, An effective electrical throughput from PANI supplement ZnS nanorods and PDMS-based flexible piezoelectric nanogenerator for power up portable electronic devices: an alternative of MWCNT filler, ACS Appl. Mater. Interfaces 7 (2015) 19091–19097.
[46] M. Pusty, L. Sinha, P.M. Shirage, A flexible self-poled piezoelectric nanogenerator based on a rGO–Ag/PVDF nanocomposite, N. J. Chem. 43 (2019) 284–294.
[47] V.F. Lvovich, Impedance Spectroscopy: Applications to Electrochemical and Dielectric Phenomena, John Wiley & Sons, 2012.
[48] N. Jalali, J. Briscoe, Y.Z. Tan, P. Woolliams, M. Stewart, P.M. Weaver, M.G. Cain, S. Dunn, ZnO nanorod surface modification with PDDA/PSS Bi-layer assembly for performance improvement of ZnO piezoelectric energy harvesting devices, J. Sol. -Gel Sci. Technol. 73 (2015) 544–549.
[49] D.D. Chung, Functional Materials: Electrical, Dielectric, Electromagnetic, Optical and Magnetic Applications, World scientific, 2021.
[50] N. Jalali, P. Woolliams, M. Stewart, P.M. Weaver, M.G. Cain, S. Dunn, J. Briscoe, Improved performance of p–n junction-based ZnO nanogenerators through CuSCN-passivation of ZnO nanorods, J. Mater. Chem. A 2 (2014) 10945–10951.